Supporting Information

Engineering metal-organic framework derived Mn-N_4-C_xS_y atomic interface for highly efficient oxygen reduction reaction

Huishan Shang,[a] Zhuoli Jiang,[a] Danni Zhou,[a] Jiajing Pei,[b] Yu Wang,[c] Juncai Dong,[d] Xusheng Zheng,[e] JiataoZhang[a] and Wenxing Chen*[a]

[a] Beijing Key Laboratory of Construction Tailorable Advanced Functional Materials and Green Applications, School of Materials Science and Engineering, Beijing Institute of Technology, Beijing 100081, China.

[b] State Key Lab of Organic-Inorganic Composites, Beijing University of Chemical Technology, Beijing 100029, China.

[c] Shanghai Synchrotron Radiation Facilities (SSRF), Shanghai Institute of Applied Physics, Chinese Academy of Science, Shanghai 201204, China.

[d] Beijing Synchrotron Radiation Facility (BSRF), Institute of High Energy Physics, Chinese Academy of Sciences, Beijing 100049, China.

[e] National Synchrotron Radiation Laboratory (NSRL), University of Science and Technology of China, Hefei 230029, China.

* Corresponding author. E-mail: wxchen@bit.edu.cn.

Table of contents

Section1: Experiment Section

Materials

Manganese (II) Acetyllacetonate ($Mn(acac)_2$, 99%, Aladdin), zinc nitrate hexahydrate (98%, Alfa Aesar), 2-methylimidazole (Acros), commercial Pt/C (20 wt% metal, Alfa Aesar), KOH (analytical grade, Sinopharm Chemical), Nafion D-521 dispersion (5% w/w in water and 1-propanol) (Alfa Aesar), L(+)-Cysteine (Aladdin), analytical grade methanol (Sinopharm Chemical), Sulphuric acid (H_2SO_4) (98%) was obtained from Beijing Chemical Reagents. N, N-dimethylformamide (DMF) (Sinopharm Chemical) were used without any further purification. The distilled water with a resistivity of 18.2 MΩ cm^{-1} was used in all experiments.

Synthesis of Samples

Preparation of Mn-ZIF-8 and pure ZIF-8: Typically, 1069mg $Zn(NO_3)_2 \cdot 6H_2O$ and 902 mg Manganese (II) Acetyllacetonate ($Mn(acac)_2$) was dissolved in 30 ml of mixture solution (DMF: methanol = 4:1) under sonication for 15 min. After that, 1161mg 2-methylimidazole (2-MeIm) was dispersed into 20 ml of mixture solution (DMF: methanol = 4:1) and was then added into the above solution immediately with vigorous stirring. Subsequently, the mixture solution was sealed for reaction at room temperature for 12 h. The as-prepared product was further collected by centrifugation and washed with methanol and finally dried at 65 °C in a vacuum oven for overnight. Pure ZIF-8 was synthesized by the same method without $Mn(acac)_2$.

Preparation of MnSAs/S-NC: A mixture of Mn-ZIF-8 and S pieces (L(+)-Cysteine) with the mass ratio 20:1 were annealed to 900 °C at a rate of 5 °C min^{-1} under an Ar gas flow and kept for 3 h and the sample was allowed to cool naturally to room temperature. Subsequently, the samples were leached in 0.5 M H_2SO_4 solution at 80 °C for 24 h to remove the free-standing metallic residues, and washed thoroughly with ethanol and deionized water. Finally, the samples were dried in vacuum at 60 ºC for overnight. MnSAs/S-NC was obtained. Additionally, MnSAs/NC was fabricated following the same process as preparing MnSAs/S-NC but without adding S pieces. S-NC was fabricated following the same process as preparing MnSAs/S-NC but with ZIF-8 as the precursor.

Characterization

The composition and structure of the as-prepared products were characterized by X-ray powder diffraction (XRD, RigakuTTR-III X-ray diffractometer with Cu Kα radiation, λ=1.5418Å). The morphologies were observed by a scanning electron microscope (SEM, JSM-6700F, 5kV) and a transmission electron microscope (TEM, JEOL JEM-2100F microscope, 200kV). The HAADF-STEM images and EDS elemental mapping were carried out in a JEOL ARM-200 microscope at 200 kV, equipped with a probe spherical aberration corrector. The samples were dispersed in ethanol and dropped onto a copper grid with a carbon film coated for TEM characterizations. The X-ray photoelectron spectroscopy (XPS) measurements were performed with an ESCA LAB 250 spectrometer on a focused monochromatic Al Kα line (1486.6 eV) X-ray beam with a diameter of 200 μm. The Mn concentration of was conducted on the inductively coupled plasma opticalemission spectrometry (ICP-OES).

Electrochemical Characterizations.

All electrochemical measurements were performed using a CHI Electrochemical Station (Model 760E) in a conventional three-electrode cell at room temperature. A glassy carbon rotating disk electrode (GC-RDE) was used as the working electrode (5 mm in diameter). The counter electrode and reference electrode were a graphite rod and saturated calomel electrode (SCE), respectively. 0.1 M KOH solution was applied as electrolyte. All potentials used in this work have been converted to the RHE scale. To prepare the catalyst ink, 1 mg catalyst powder was dispersed in 1 mL solution containing 750 μL isopropyl alcohol, 250 μL deionized water and 20 μL 5% Nafion solution by sonication for at least 1 h. Then a certain volume of the catalyst ink was droped on the surface of the glassy carbon electrode with the catalyst loading 0.102 mg cm^{-2} and then dried under room temperature. Before ORR tests, N_2/O_2 flow was carried out through the electrolyte in the cell for about 30 min and a flow of O_2 was maintained over the electrolyte during the measurements to ensure O_2 saturation. The cyclic voltammetry (CV) tests of the catalyst under N_2- and O_2-saturated alkaline electrolyte were performed with a scan rate of 50 mV s^{-1}. The Linear sweep voltammetry (LSV) of the catalyst was measured in O_2-saturated KOH (0.1 M) water solution with varying rotating speed from 400 to 2500 rpm. Rotating ring-disk electrode (RRDE) measurements was carried out to determine the four-electron selectivity. The electrolytes were 0.1 M KOH and the disk electrode was scanned at a rate of 10 mV s^{-1}, and the ring electrode potential was set to 1.23 V vs. RHE.

Electrochemical data processing

The Tafel slopes were calculated according to the Tafel equation η= b log (j/j_0) based on the LSV curves, where η is the overpotential, b is the Tafel slope, j is the current density, and j_0 is the exchange current density.

The number of electrons transferred (n) and kinetic current density (J_K) during ORR were calculated according to Koutecky-Levich equation:

$$\frac{1}{J}=\frac{1}{J_L}+\frac{1}{J_K}=\frac{1}{B\omega^{0.5}}+\frac{1}{J_K}$$

$$B=0.62nFC_0D_0^{\frac{2}{3}}V^{-\frac{1}{6}}$$

where J is the measured current density, J_K and J_L are the kinetic and limiting current densities, ω is the angular velocity of the disk, n is the overall number of electrons transferred in oxygen reduction, F is the Faraday constant (96485 C mol^{-1}), C_0 is the bulk concentration of O_2 (1.2×10^{-6} mol cm^{-3}), D_0 is the diffusion coefficient of O_2 in 0.1 M KOH (1.9×10^{-5} cm^2 s^{-1}), and V is the kinematic viscosity of the electrolyte (0.01 cm^2 s^{-1}), and k is the electron transfer rate constant.

The Hydrogen peroxide yield (%H_2O_2) and the electron transfer number (n) were determined by the following equations:

$$H_2O_2(\%)=\frac{200\times I_r}{N\times I_d+\ I_r}$$

$$n=\frac{4\times I_d}{I_d+\dfrac{I_r}{N}}$$

where I_r and I_d are ring and disk currents, and N is collection efficiency (0.37).

Soft-XAS measurements

The soft XANES spectra (C K-edge, N K-edge a) were measured at beamline BL12B of National Synchrotron Radiation Laboratory (NSRL). A bending magnet is connected to the beamline, which is equipped with three gratings covering photon energy range from 100 to 1000 eV with an energy resolution of ~0.2 eV. The resolving power of the grating was typically E/ΔE

= 1000, and the photon flux was 1× 10^{-10} photons per second. All the samples for solf XAS test were deposited onto double-sided carbon tape and the data were recorded in the total electron yield mode.

XAFS measurements

The XAFS spectra data (Mn K-edge) were collected at BL14W1 station in Shanghai Synchrotron Radiation Facility (SSRF, operated at 3.5 GeV with a maximum current of 250 mA). The XAFS data of the samples were collected at room temperature in fluorescence excitation mode using a Lytle detector.

The cell for operando XAS measurement possesses transparent flat walls with a single circular hole (1.5 cm in diameter). The MnSAs/S-NC coated carbon paper with the catalyst layer facing inward was contacted with a copper conductor. 0.1 M KOH solution was poured into the cell (O_2-saturated), without stirring during all the experiments. A cap fitted with reference and counter electrodes was employed to cover the cell and ensure a fixed distance between the three electrodes during the measurements. Before the operando XAS measurements, the spectra were recorded at different positions on the working electrode to check the homogeneity of the catalyst. At each potential, three scans were collected at the Mn K-edge. After each potential change, the system was allowed to equilibrate for 20 min before the recording of a next spectrum.

XAFS Data Processing

The acquired EXAFS data were processed according to the standard procedures using the Athena and Artemis implemented in the IFEFFIT software packages. The fitting detail is described below:

The acquired EXAFS data were processed according to the standard procedures using the ATHENA module implemented in the IFEFFIT software packages. The EXAFS spectra were obtained by subtracting the post-edge background from the overall absorption and then normalizing with respect to the edge-jump step. Subsequently, the χ(k) data of were Fourier transformed to real (R) space using a hanning windows (dk=1.0 $Å^{-1}$) to separate the EXAFS contributions from different coordination shells. To obtain the quantitative structural parameters around central atoms, least-squares curve parameter fitting was performed using the ARTEMIS module of IFEFFIT software packages.

The following EXAFS equation was used:

$$\chi(k)=\sum_j \frac{N_j S_o^2 F_j(k)}{k R_j^2}\exp[-2k^2\sigma_j^2]\exp[\frac{-2R_j}{\lambda(k)}]\sin[2kR_j+\phi_j(k)]$$

S_0^2 is the amplitude reduction factor, $F_j(k)$ is the effective curved-wave backscattering amplitude, N_j is the number of neighbors in the j^{th} atomic shell, R_j is the distance between the X-ray absorbing central atom and the atoms in the j^{th} atomic shell (backscatterer), λ is the mean free path in Å, $\phi_j(k)$ is the phase shift (including the phase shift for each shell and the total central atom phase shift), σ_j is the Debye-Waller parameter of the j^{th} atomic shell (variation of distances around the average R_j). The functions $F_j(k)$, λ and $\phi_j(k)$ were calculated with the ab initio code FEFF8.2. The coordination numbers of model samples were fixed as the nominal values. The obtained S_0^2 was fixed in the subsequent fitting. While the internal atomic distances R, Debye-Waller factor σ^2, and the edge-energy shift ΔE_0 were allowed to run freely.

Section2: Supporting figures and tables

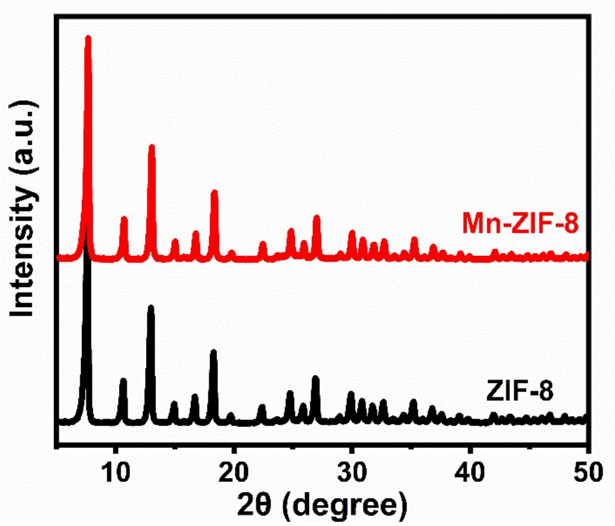

Fig. S1. XRD patterns of pure ZIF-8 and Mn-ZIF-8.

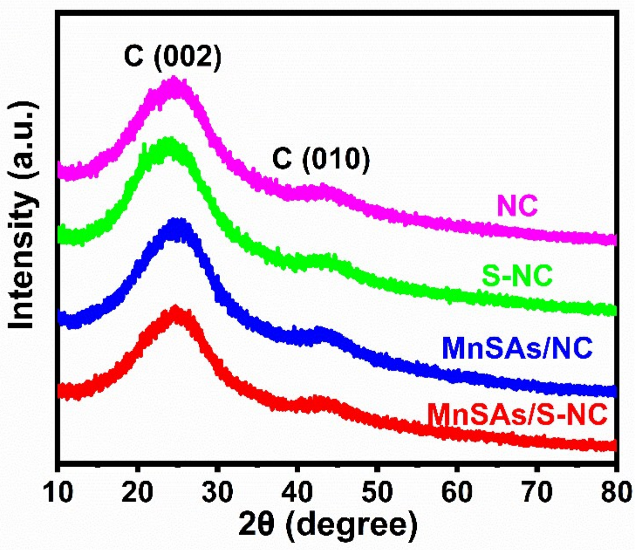

Fig. S2. XRD patterns of NC, S-NC, MnSAs/NC and MnSAs/S-NC.

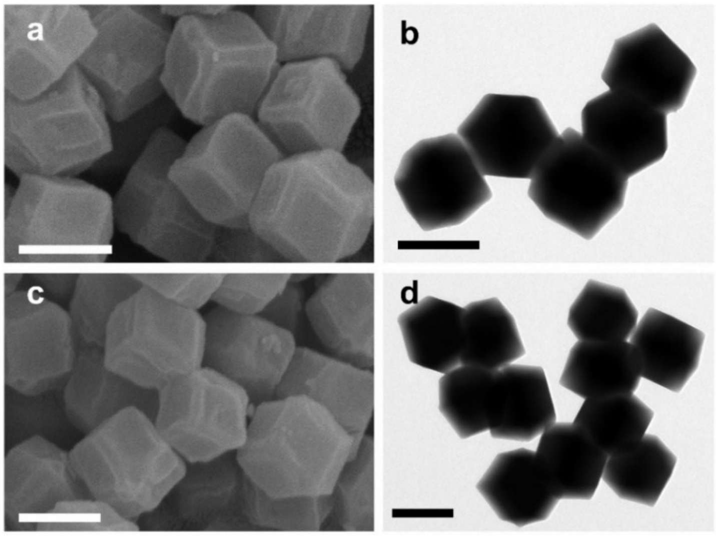

Fig. S3. SEM and TEM images of (a, b) ZIF-8 and (c, d) Mn-ZIF-8. The scale bar is 200 nm.

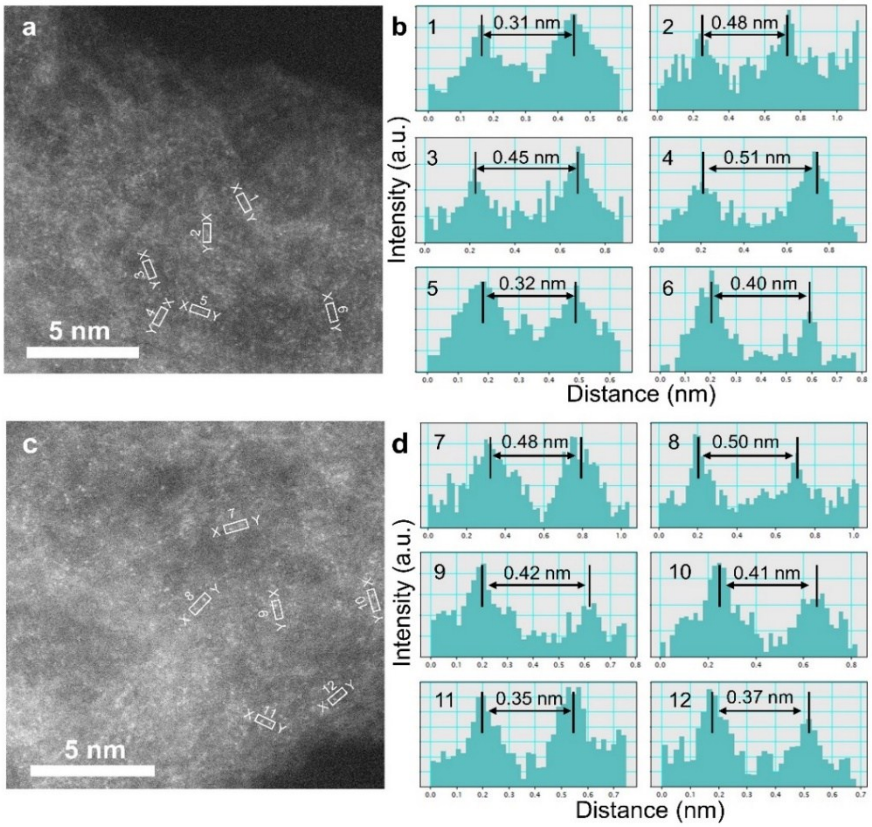

Fig. S4. A distribution of gaps between the single atoms over a larger area. (a) and (c) HAADF-STEM images of MnSAs/S-NC catalyst. (b) and (d) The corresponding intensity profiles along the line X-Y in a and c, respectively.

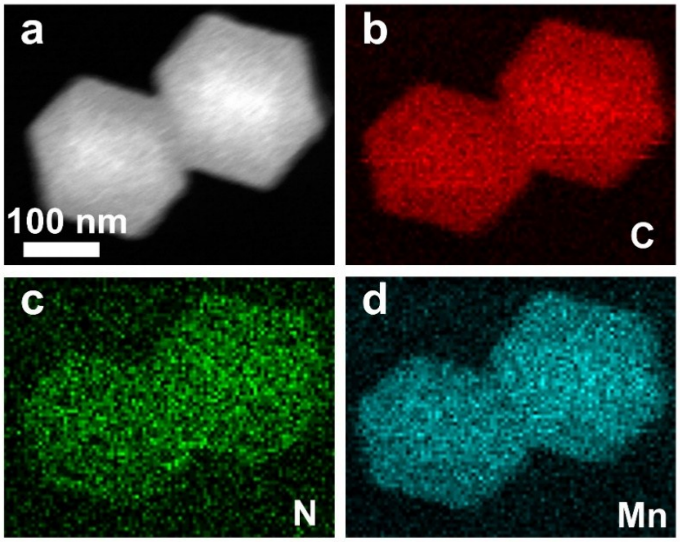

Fig. S5. (a) STEM images of MnSAs/NC (b-d) EDS images, C (red), N (green), and Mn (cyan).

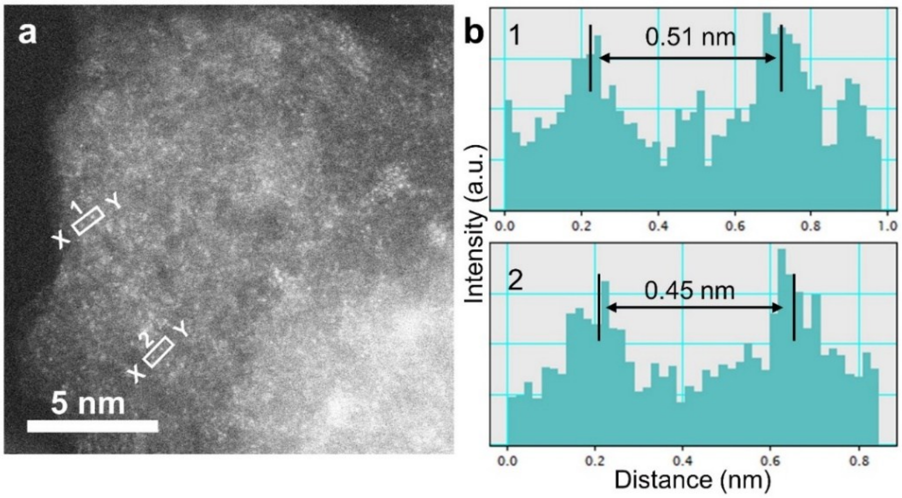

Fig. S6. (a) HAADF-STEM images of MnSAs/NC. (b) The corresponding intensity profiles along the line X-Y in a.

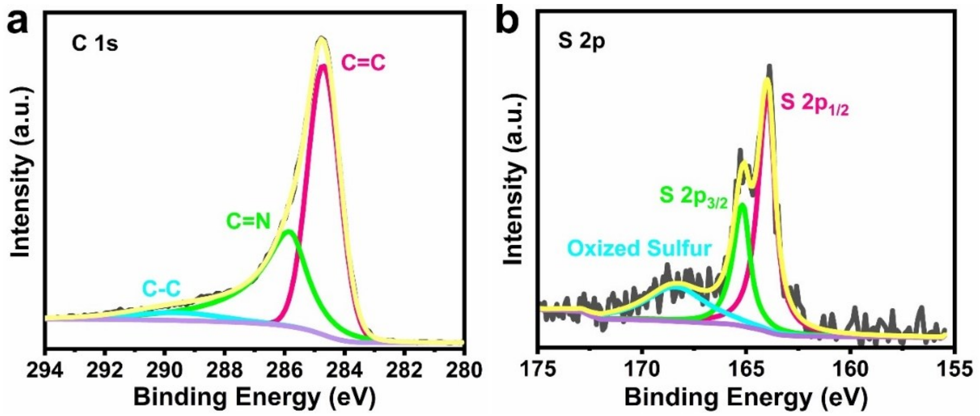

Fig. S7. The XPS spectra for (a) C 1s and (b) S 2p region of MnSAs/S-NC.

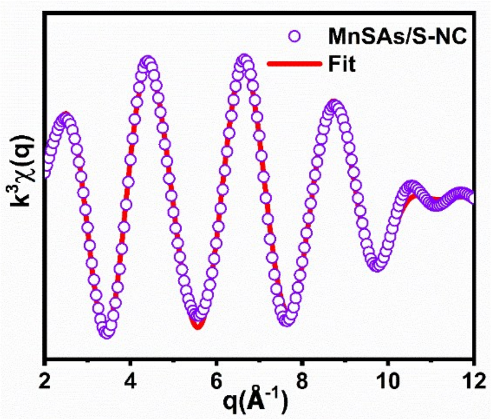

Fig. S8. The q space EXAFS fitting curve at Mn K-edge of MnSAs/S-NC.

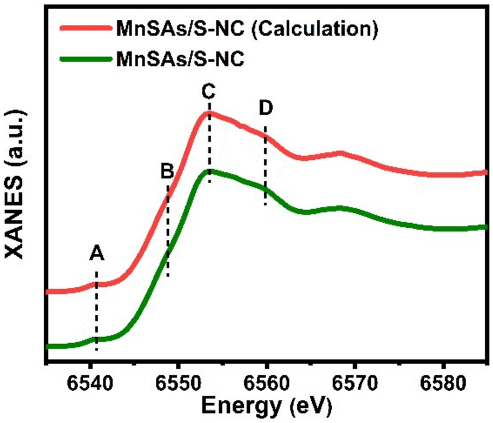

Fig. S9. Experimental XANES and calculated XANES curves of MnSAs/S-NC at Mn K-edge.

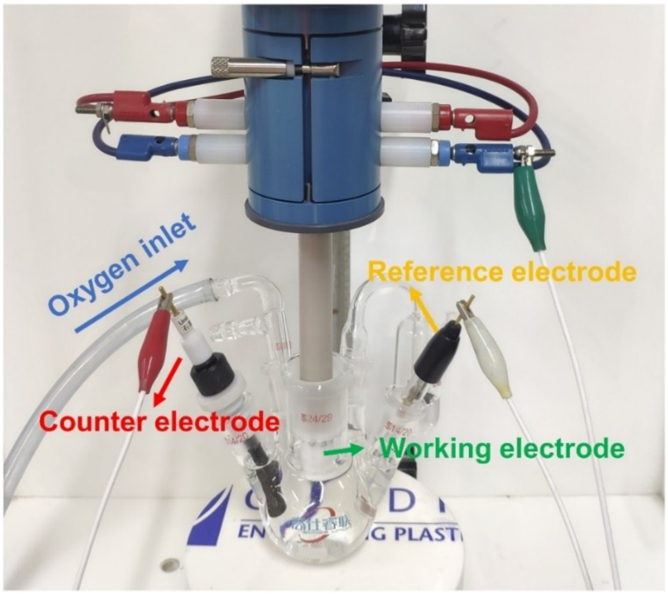

Fig. S10. Photograph of the typical three-electrode setup for the electrochemical ORR measurements

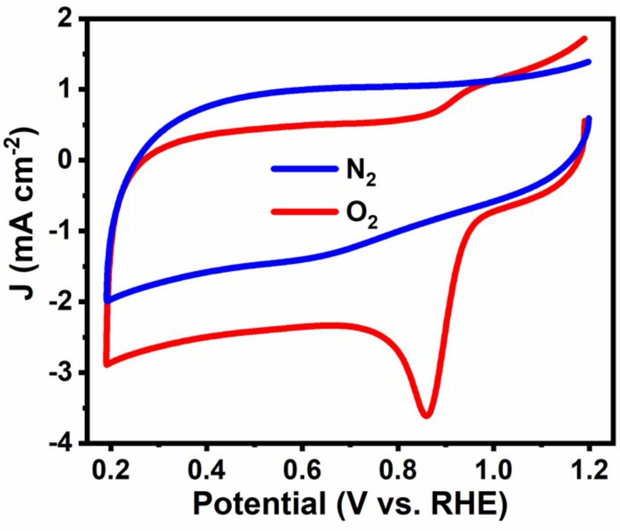

Fig. S11. CV curves of MnSAs/S-NC in O_2- and N_2-saturated 0.1M KOH electrolyte at a scan rate of 50 mV/s.

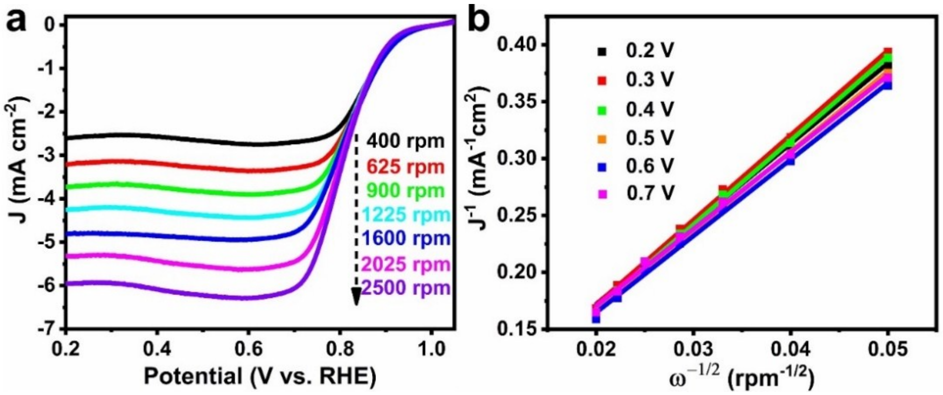

Fig. S12. (a) LSV curves of Pt/C in O_2-saturated 0.1 M KOH at 400-2500 rpm. (b) The corresponding K–L plots at various potentials.

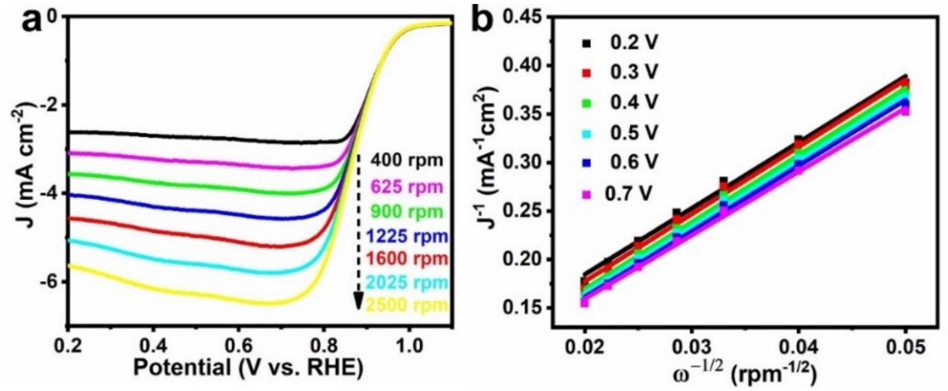

Fig. S13. (a) LSV curves of MnSAs/NC in O_2-saturated 0.1 M KOH at 400-2500 rpm. (b) The corresponding K–L plots at various potentials.

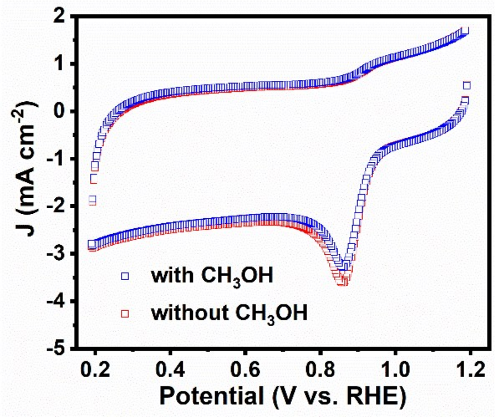

Fig. S14. Cyclic voltammetry (CV) data for MnSAs/S-NC in O_2-saturated 0.1 M KOH without and with 0.5 M CH_3OH.

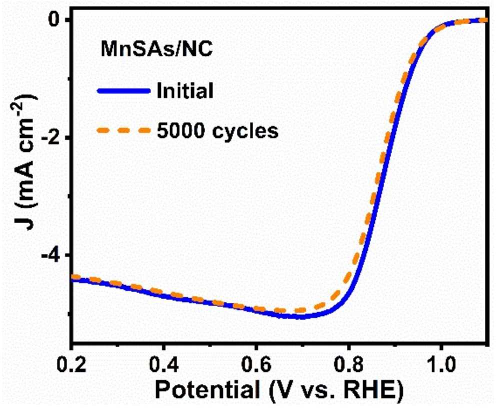

Fig. S15. ORR polarization curves of MnSAs/NC before and after 5000 potential cycles in 0.1M KOH.

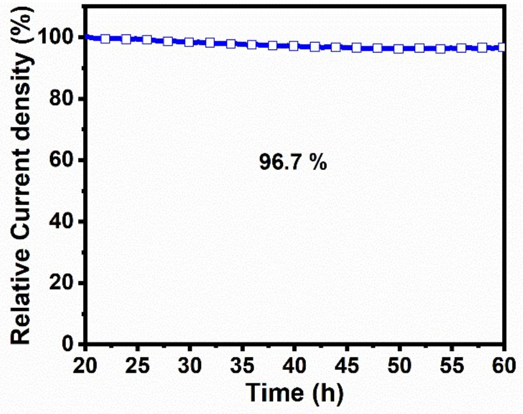

Fig. S16. Chronoamperometric response at 0.90 V for MnSAs/S-NC.

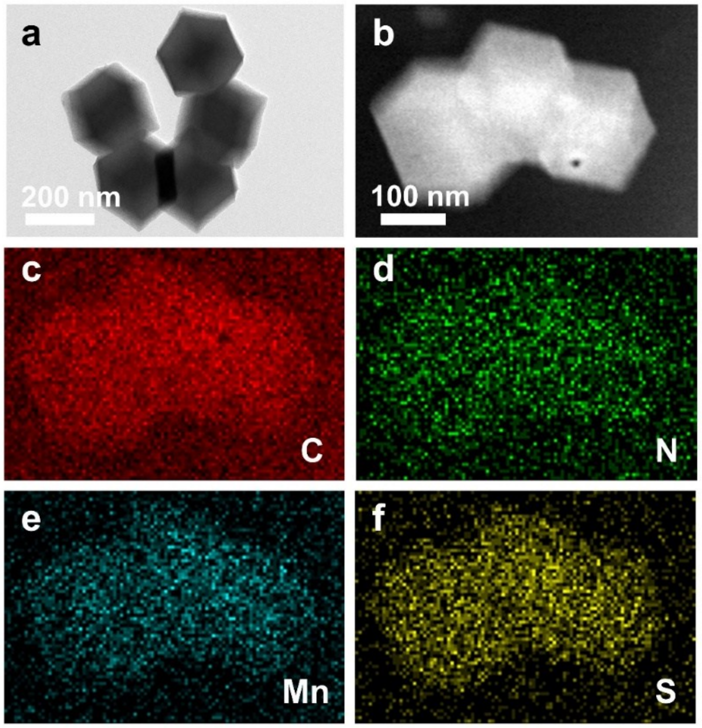

Fig. S17. (a) TEM, (b) STEM, (c-f) EDS images of MnSAs/S-NC catalyst after durability test.

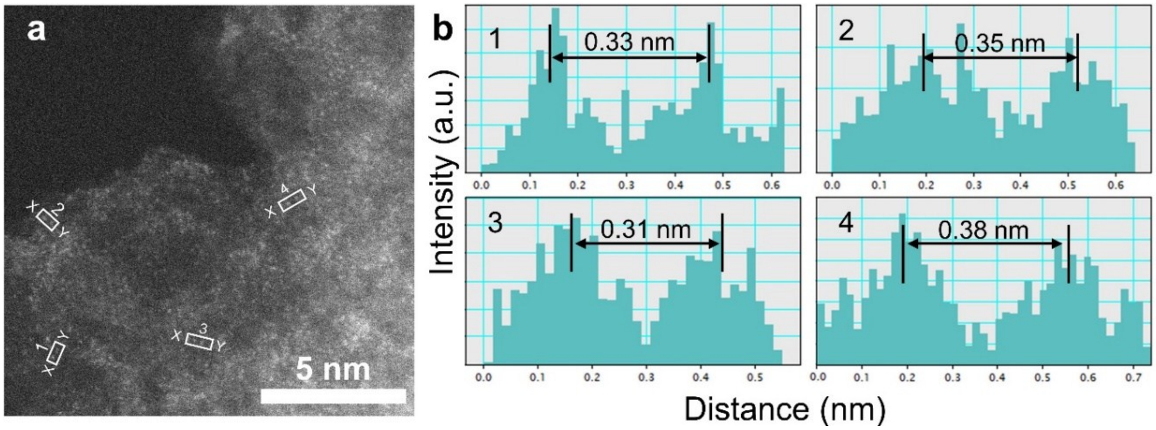

Fig. S18. (a) HAADF-STEM images of MnSAs/S-NC catalyst after durability test. (b) The corresponding intensity profiles along the line X-Y in a.

We evaluated the ORR performance of the MnSAs/S-NC catalyst in 0.5 M H_2SO_4 solution. Fig. S19a showed the ORR polarization curves of different catalysts. The half-wave potential ($E_{1/2}$) of MnSAs/S-NC exhibited 0.73 V *vs.* RHE, which was 30 mV higher than MnSAs/NC. As we could see, MnSAs/S-NC showed comparable ORR activity in acid conditions, related to Fe-N-C and Co-N-C catalysts in the literatures (Table S3). The ORR kinetics of MnSAs/S-NC was evaluated by the Tafel plots. In Fig. S19b, MnSAs/S-NC showed low Tafel slope of 98.7 mV dec^{-1}, which demonstrated the favorable ORR kinetics. The ORR polarization curves of MnSAs/S-NC under different rotating speed was exhibited in Fig. S19c. The derived Koutecky-Levich (K-L) plots in Fig. S19d illustrated MnSAs/S-NC in acidic condition followed high-efficiency four-electron ORR process.

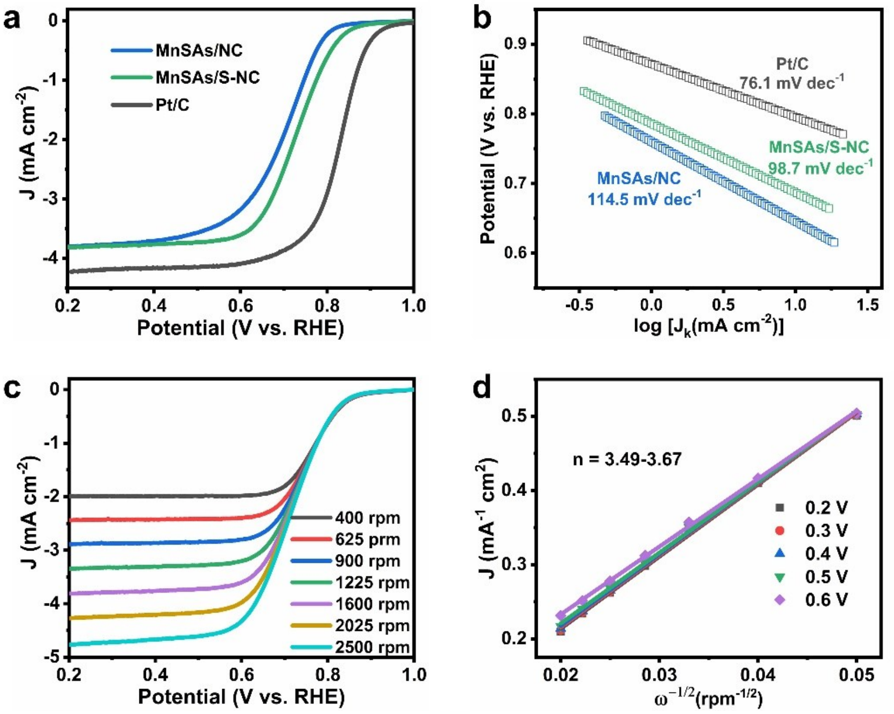

Fig. S19. (a) Polarization curves for MnSAs/S-NC, MnSAs/NC in 0.5 M H_2SO_4 solution and commercial Pt/C in 0.1 M $HClO_4$ solution. (b) The corresponding Tafel plots for MnSAs/S-NC, MnSAs/NC and Pt/C. (c) The ORR polarization curves of MnSAs/S-NC at different rotating speed. (d) The K-L plots of MnSAs/S-NC.

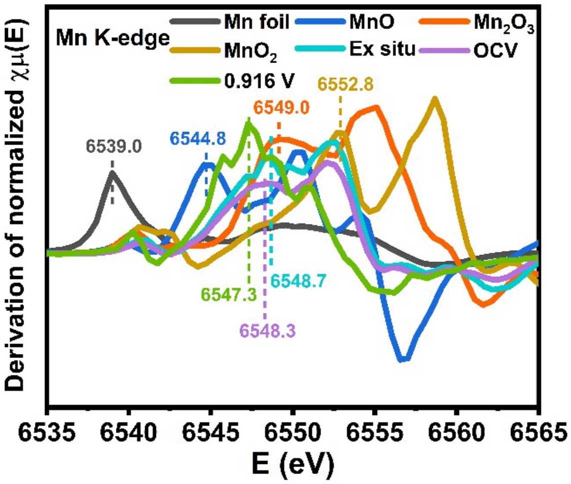

Fig. S20. First-derivative XANES curves of MnSAs/S-NC and the references.

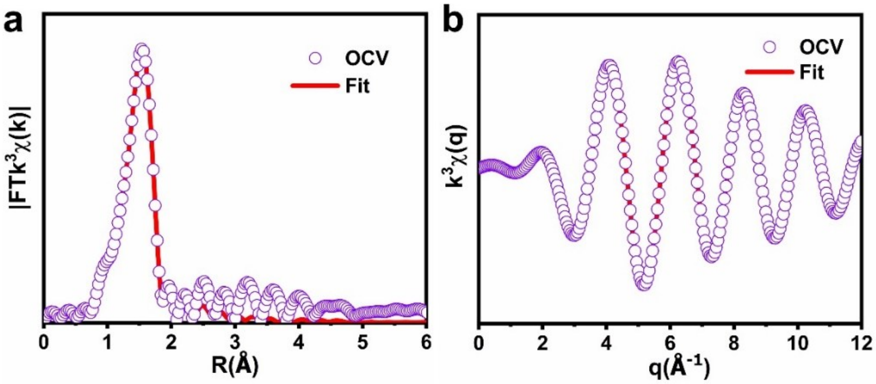

Fig. S21. EXAFS fitting curves of MnSAs/S-NC at OCV.

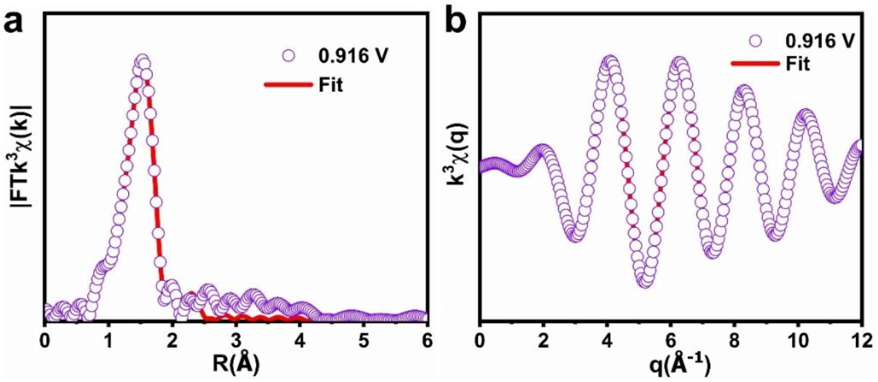

Fig. S22. EXAFS fitting curves of MnSAs/S-NC at 0.916 V *vs.* RHE.

In Fig. S23, from 0.916 V *vs.* RHE to OCV, the Mn-N peaks displayed a slightly low-R shift from 1.59 Å to 1.53 Å. Quantitatively, the EXAFS fitting suggested that the mean bond length for Mn-N under the catalytic condition decreased from 2.02 Å (0.916 V) to 1.98 Å (OCV) (Fig. S24-S25 and Table S5).

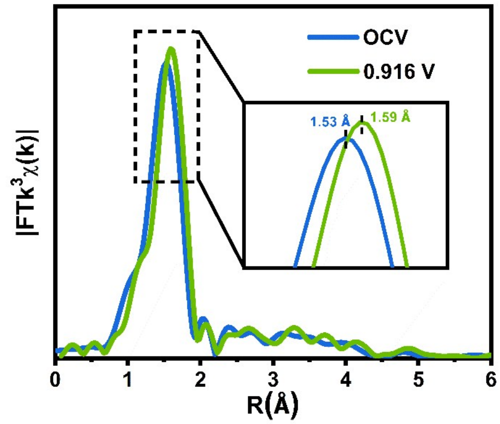

Fig. S23. Mn K-edge EXAFS spectra of MnSAs/S-NC at various potentials during reversal tests.

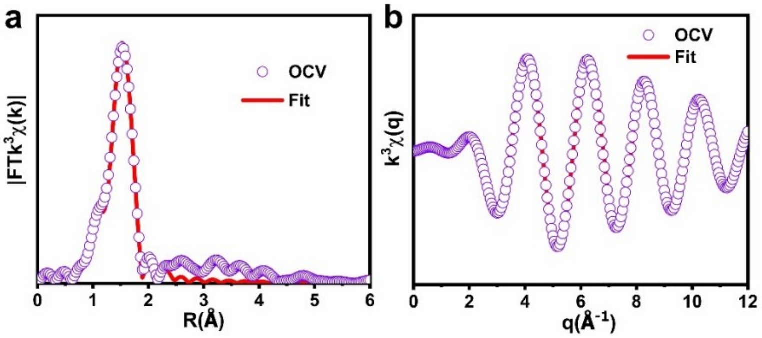

Fig. S24. EXAFS fitting curves of MnSAs/S-NC at 0.916 V *vs.* RHE during reversal tests.

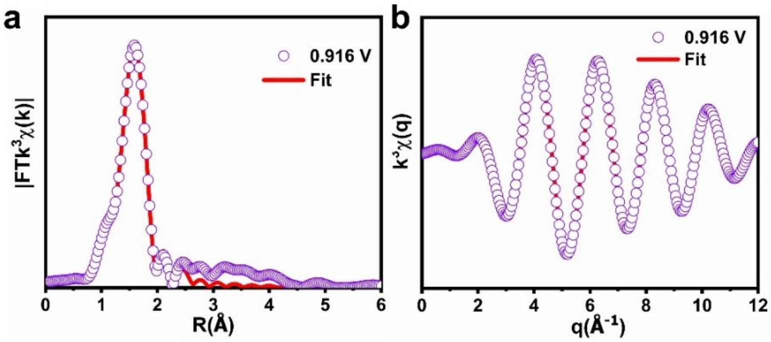

Fig. S25. EXAFS fitting curves of MnSAs/S-NC at OCV during reversal tests.

The XAS data of Mn-N-C without S (MnSAs/NC) was added. The EXAFS fitting results were exhibited in (Fig. S26 and Table S6), which showed that the Mn atom was coordinated by four N atoms at the first shell with bond length of 1.96 Å, suggesting the formation of Mn-N_4 configuration. The operando experiment of MnSAs/NC was also performed. The XAFS were recorded at the OCV and the potential of $E_{1/2}$. Fig. S27 presented the XANES spectra at the Mn K-edge of MnSAs/NC collected at different conditions, along with the data of Mn foil, MnO, Mn_2O_3 and MnO_2 as standards. From the dry sample to OCV and then to $E_{1/2}$, the position of absorption edge was just slightly shifted. Fig. S28 showed the k^3-weighted FT-EXAFS spectra for MnSAs/NC at different applied potentials. The FT curves still exhibited one main peak, assigned to Mn-N coordination. However, the Mn-N peaks displayed a slightly high-R shift from 1.52 Å to 1.54 Å. Quantitatively, the EXAFS curve-fitting for the first coordination shell was carried out. The mean bond length for Mn-N under the catalytic condition increased from 1.97 Å (OCV) to 2.00 Å ($E_{1/2}$) (Fig. S29-S30 and Table S6).

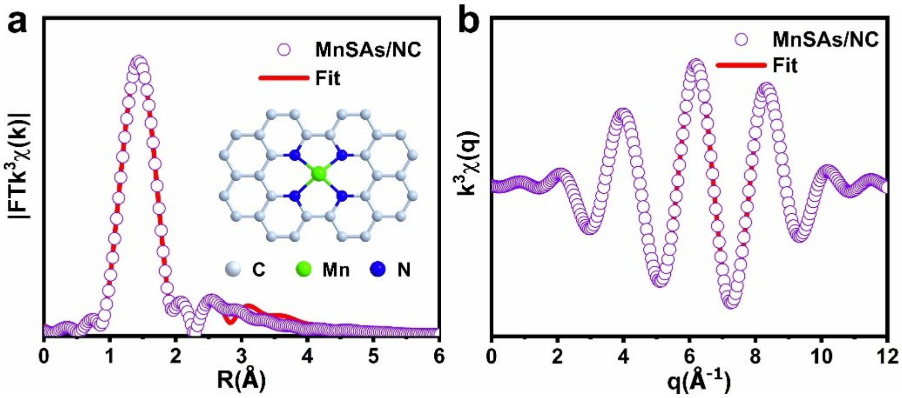

Fig. S26. EXAFS fitting curves of MnSAs/NC at Mn K-edge.

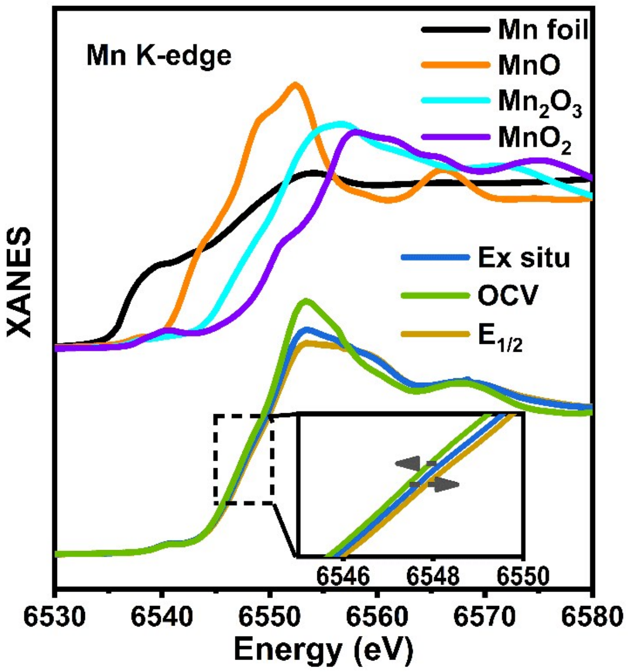

Fig. S27. Operando XANES spectra recorded at the Mn K-edge of MnSAs/NC from the OCV condition to $E_{1/2}$ during electrocatalytic ORR.

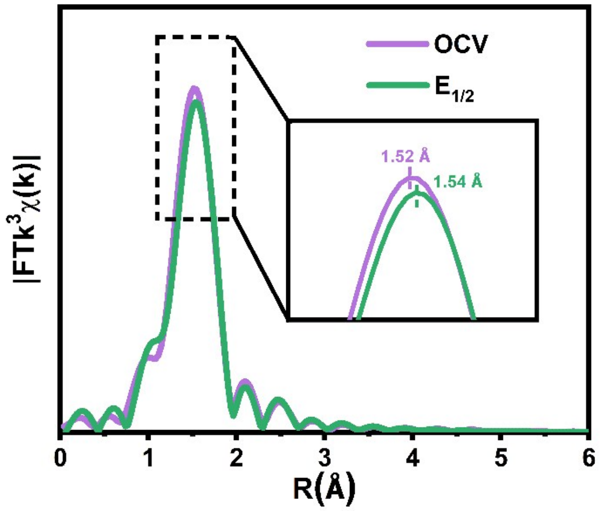

Fig. S28. Mn K-edge EXAFS spectra of MnSAs/NC at various potentials during ORR.

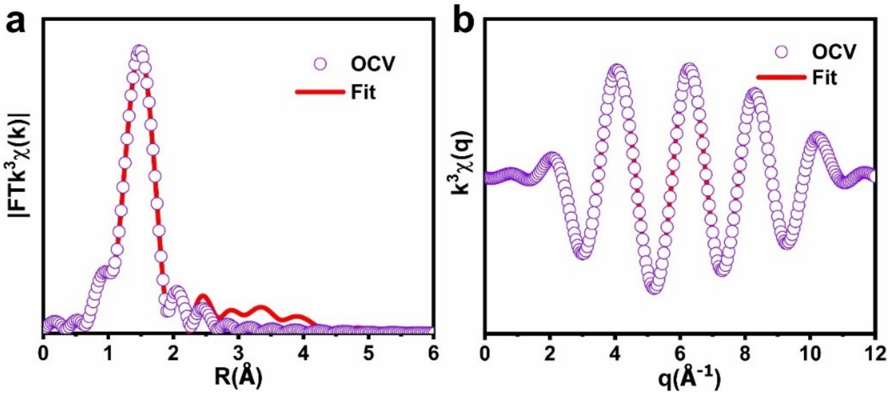

Fig. S29. EXAFS fitting curves of MnSAs/NC at OCV.

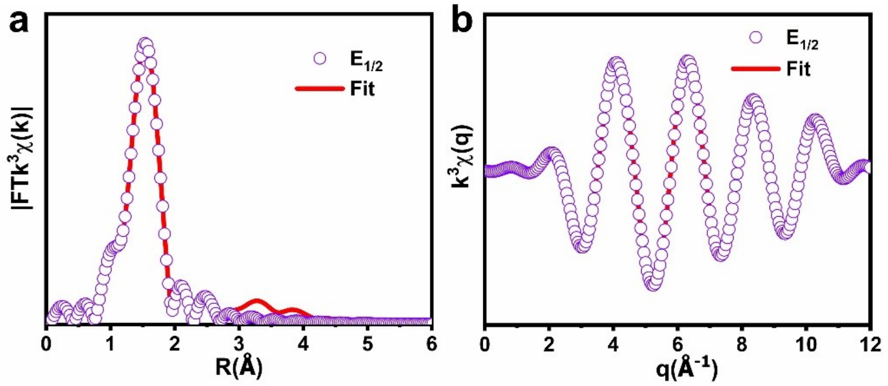

Fig. S30. EXAFS fitting curves of MnSAs/NC at $E_{1/2}$.

Table S1. Structural parameters extracted from the Mn K-edge EXAFS fitting. (S_0^2=0.85).

Sample	**Scattering pair**	**CN**	**R(Å)**	**$\sigma^2(10^{-3}Å^2)$**	**ΔE_0(eV)**	**R factor**
MnSAs/S-NC	Mn-N	4.2	1.98	5.6	0.5	0.007

S_0^2 is the amplitude reduction factor; CN is the coordination number; R is interatomic distance (the bond length between Ru central atoms and surrounding coordination atoms); σ^2 is Debye-Waller factor (a measure of thermal and static disorder in absorber-scatterer distances); ΔE_0 is edge-energy shift (the difference between the zero kinetic energy value of the sample and that of the theoretical model). R factor is used to value the goodness of the fitting.

Error bounds that characterize the structural parameters obtained by EXAFS spectroscopy were estimated as N ± 20%; R ± 1%; σ^2 ± 20%; ΔE_0 ± 20%.

Table S2. ORR parameters for recently reported non-precious single atom catalysts in alkaline electrolyte

	Electrocatalysts	**Onset potential (V vs. RHE)**	**Half-wave potential (V vs. RHE)**	**loading (mg cm-2)**	**Reference**
	MnSAs/S-NC	**1.04**	**0.916**	**0.102**	**This work**
1	FeSA-N-C	1.00	0.89	0.28	*Angew. Chem. Int. Ed.,* 2018, **57**, 8525-8529
2	S,N-Fe/N/C-CNT	0.94	0.85	0.6	*Angew. Chem. Int. Ed.,* 2017, **56**, 610-614.
3	Cu SAs/N-C	~1	0.895	0.09	*Nat. Catal.*, 2018, **1**, 781-786.
4	Fe-ISA/SNC	0.97	0.896	0.510	*Adv. Mater.,* 2018, **30**, 1800588.
5	Mn/C-NO	0.94	0.86	0.300	*Adv. Mater.,* 2018, **30**, 1801732.
6	Co-ISAS/p-CN	0.92	0.838	-	*Adv. Mater.,* 2018, **30**, 1706508.
7	Fe/SNC	0.96	0.86	0.51	*Angew. Chem. Int. Ed.,* 2017, **56**, 13800-13804.
8	SA-Fe-HPC	0.96	0.89	-	*Angew. Chem. Int. Ed.,* 2018, **57**, 9038-9043.
9	Co-POC	0.9	0.83	0.100	*Adv. Mater.,* 2019, **31**, 1900592.
10	SA-Fe/NG	1.00	0.88	0.6	*PNAS* 2018, **115**, 6626-6631.
11	Cu-N-C	0.98	0.869	3.31	*Energy Environ. Sci.,* 2018, **11**, 2263-2269.
12	Fe-NC SAC	0.98	0.90	0.6	*Nat. Commun.,* 2019, **10**, 1278.
13	Fe-N/P-C-700	0.941	0.867	0.6	*J. Am. Chem. Soc.,* 2020, **142**, 5, 2404-2412.
14	Zn/CoN-C	1.004	0.861	0.225	*Angew. Chem.,* 2019, **131**, 2648-2652.

Table S3. Comparison of ORR performance between MnSAs/S-NC and other M-N-C catalysts reported in the literatures under acid media.

Electrocatalysts	**Electrolyte**	**Onset potential (V vs. RHE)**	**Half-wave potential (V vs. RHE)**	**Reference**
MnSAs/S-NC	**0.5M H_2SO_4**	**0.88**	**0.73**	**This work**
Fe/SNC	0.5M H_2SO_4	0.89	0.77	*Angew. Chem. Int. Ed.,* 2017*,* **56**, 13800-13804.
Fe-N-CNF	0.5M H_2SO_4	0.84	0.62	*Angew. Chem. Int. Ed.,* 2015*,* **54**, 8179.
Fe−N/C-800	0.1M $HClO_4$	0.82	0.6	*J. Am. Chem. Soc.,* 2014*,* **136**, 11027-11033.
Fe-CNT/PC	0.1M $HClO_4$	0.95	0.79	*J. Am. Chem. Soc.,* 2016*,* **138***, 15046-15056.*
CPANI-Fe-NaCl	0.1M $HClO_4$	0.88	0.73	*J. Am. Chem. Soc.,*2015, **137**, 5414-5420.
FeCo/C-800	0.1M $HClO_4$	0.90	0.76	*Adv. Mater.,* 2015, **27**, 3431-3436.
Co-N-C	0.1M H_2SO_4	~0.92	~0.76	*Nat. Commun.,* 2017, **8**, 957.
Co-N-C	0.1M $HClO_4$	0.88	0.76	*ACS Catal.* 2015*,* **5**, 7068-7076.
Co-N/CNFs	0.1M $HClO_4$	0.82	0.70	*ACS Catal.* 2017, **7**, 6864-6871.
Co-N-C	0.1M $HClO_4$	0.89	0.73	*Small* 2018, **14**, 1704319.

Table S4. Structural parameters extracted from the Mn K-edge EXAFS fitting under catalytic conditions. (S_0^2=0.85).

Sample	**Scattering pair**	**CN**	**R(Å)**	**$\sigma^2(10^{-3}Å^2)$**	**ΔE_0(eV)**	**R factor**
MnSAs/S-NC (OCV)	Mn-N	4.0	1.99	5.1	0.5	0.007
	Mn-O	1.1	2.04	5.7	1.0	0.009
MnSAs/S-NC (0.916 V)	Mn-N	3.9	2.02	5.4	0.5	0.005
	Mn-O	1.2	2.04	6.1	1.0	0.007

S_0^2 is the amplitude reduction factor; CN is the coordination number; R is interatomic distance (the bond length between Ru central atoms and surrounding coordination atoms); σ^2 is Debye-Waller factor (a measure of thermal and static disorder in absorber-scatterer distances); ΔE_0 is edge-energy shift (the difference between the zero kinetic energy value of the sample and that of the theoretical model). R factor is used to value the goodness of the fitting.

Error bounds that characterize the structural parameters obtained by EXAFS spectroscopy were estimated as N ± 20%; R ± 1%; σ^2 ± 20%; ΔE_0 ± 20%.

Table S5. Structural parameters extracted from the Mn K-edge EXAFS fitting under catalytic conditions. (S_0^2=0.85).

Sample	**Scattering pair**	**CN**	**R(Å)**	**$\sigma^2(10^{-3}Å^2)$**	**ΔE_0(eV)**	**R factor**
MnSAs/S-NC (0.916 V)-reversal	Mn-N	4.0	2.02	5.6	1.0	0.006
	Mn-O	0.9	2.03	6.4	1.0	0.005
MnSAs/S-NC (OCV)-reversal	Mn-N	3.8	1.98	5.8	1.0	0.007
	Mn-O	1.0	2.04	6.3	1.0	0.008

S_0^2 is the amplitude reduction factor; CN is the coordination number; R is interatomic distance (the bond length between Ru central atoms and surrounding coordination atoms); σ^2 is Debye-Waller factor (a measure of thermal and static disorder in absorber-scatterer distances); ΔE_0 is edge-energy shift (the difference between the zero kinetic energy value of the sample and that of the theoretical model). R factor is used to value the goodness of the fitting.

Error bounds that characterize the structural parameters obtained by EXAFS spectroscopy were estimated as N ± 20%; R ± 1%; σ^2 ± 20%; ΔE_0 ± 20%.

Table S6. Structural parameters extracted from the Mn K-edge EXAFS fitting under catalytic conditions. (S_0^2=0.85).

Sample	**Scattering pair**	**CN**	**R(Å)**	**$\sigma^2(10^{-3}Å^2)$**	**ΔE_0(eV)**	**R factor**
MnSAs/NC (ex situ)	Mn-N	4.1	1.96	4.9	0.5	0.005
MnSAs/NC ($E_{1/2}$)	Mn-N	4.0	1.97	5.5	0.5	0.006
	Mn-O	1.0	2.03	5.8	1.5	0.007
MnSAs/NC (OCV)	Mn-N	3.8	2.00	6.1	1.0	0.008
	Mn-O	1.1	2.03	6.6	1.0	0.007

S_0^2 is the amplitude reduction factor; CN is the coordination number; R is interatomic distance (the bond length between Ru central atoms and surrounding coordination atoms); σ^2 is Debye-Waller factor (a measure of thermal and static disorder in absorber-scatterer distances); ΔE_0 is edge-energy shift (the difference between the zero kinetic energy value of the sample and that of the theoretical model). R factor is used to value the goodness of the fitting.

Error bounds that characterize the structural parameters obtained by EXAFS spectroscopy were estimated as N ± 20%; R ± 1%; σ^2 ± 20%; ΔE_0 ± 20%.

References

1. H. Jiang, L. Jiao, G. Wan, R. Zhang, S. Yu, *Angew. Chem. Int. Ed.*, 2018, **57**, 8525-8529.

2. P. Chen, T. Zhou, L. Xing, K. Xu, Y. Tong, H. Xie, Y. Xie, *Angew. Chem. Int. Ed.,* 2017, **56**, 610-614.

3. Y. Qu, Z. Li, W. Chen, Y. Wu, Y. Li, *Nat. Catal.,* 2018, **1**, 781-786.

4. Q. Li, W. Chen, H. Xiao, Y. Gong, Z. Li, L. Zheng, Y. Li, *Adv. Mater.,* 2018, **30**, 1800588.

5. Y. Yang, K. Mao, S. Gao, H. Huang, G. Xia, Z. Lin, Q. Chen, *Adv. Mater.,* 2018, **30**, 1801732.

6. A. Han, W. Chen, S. Zhang, M. Zhang, Y. Han, J. Zhang, Y. Li, *Adv. Mater.,* 2018, **30**, 1706508.

7. H. Shen, E. Graciaespino, J. Ma, K. Zang, J. Luo, L. Wang, S. Guo, *Angew. Chem. Int. Ed.,* 2017, 56, 13800-13804.

8. Z. Zhang, J. Sun, F. Wang, L. Dai, *Angew. Chem. Int. Ed.,* 2018, **57**, 9038-9043.

9. B. Li, C. Zhao, S. Chen, J. Liu, X. Chen, L. Song, Q. Zhang, *Adv. Mater.,* 2019, **31**, 1900592.

10. L. Yang, D. Cheng, H. Xu, X. Zeng, X. Wan, J. Shui, D. Cao, *PNAS*, 2018,**115**, 6626-6631.

11. F. Li, G. Han, H. Noh, S. Kim, Y. Lu, H. Y. Jeong, J. Baek, *Energy Environ. Sci.,* 2018, **11**, 2263-2269.

12. L. Zhao, Y. Zhang, L. Huang, X. Liu, Q. Zhang, C. He, L. Wan, *Nature Commun.*, 2019, **10**, 1278.

13. K. Yuan, D. Lutzenkirc-Henhecht, L. Li, L. Shuai, Y. Li, R. Cao, U. Scherf, *J. Am. Chem. Soc.*, 2020, **142**, 5, 2404-2412.

14. Z. Lu, B. Wang, Y. Hu, W. Liu, Y. Zhao, R. Yang, X. Sun, *Angew. Chem.,* 2019, 131, 2648-2652.